# Oligoethylene Glycol Side Chains Increase Charge Generation in Organic Semiconductor Nanoparticles for Enhanced Photocatalytic Hydrogen Evolution

*Jan Kosco,\* Soranyel Gonzalez-Carrero, Calvyn T. Howells, Weimin Zhang,
Maximilian Moser, Rajendar Sheelamanthula, Lingyun Zhao, Benjamin Willner,
Tania C. Hidalgo, Hendrik Faber, Balaji Purushothaman, Michael Sachs,
Hyojung Cha, Rachid Sougrat, Thomas D. Anthopoulos, Sahika Inal,
James R. Durrant, and Iain McCulloch\**

Organic semiconductor nanoparticles (NPs) composed of an electron donor/acceptor (D/A) semiconductor blend have recently emerged as an efficient class of hydrogen-evolution photocatalysts. It is demonstrated that using conjugated polymers functionalized with (oligo)ethylene glycol side chains in NP photocatalysts can greatly enhance their $H_2$-evolution efficiency compared to their nonglycolated analogues. The strategy is broadly applicable to a range of structurally diverse conjugated polymers. Transient spectroscopic studies show that glycolation facilitates charge generation even in the absence of a D/A heterojunction, and further suppresses both geminate and nongeminate charge recombination in D/A NPs. This results in a high yield of photogenerated charges with lifetimes long enough to efficiently drive ascorbic acid oxidation, which is correlated with greatly enhanced $H_2$-evolution rates in the glycolated NPs. Glycolation increases the relative permittivity of the semiconductors and facilitates water uptake. Together, these effects may increase the high-frequency relative permittivity inside the NPs sufficiently, to cause the observed suppression of exciton and charge recombination responsible for the high photocatalytic activities of the glycolated NPs.

## 1. Introduction

Solar irradiation is an abundant source of renewable energy. However, the conversion of solar energy into a form that can be stored and used on demand remains a major challenge. Photocatalytic water splitting to generate hydrogen; a versatile, clean burning fuel, is a potential solution to this problem.[1] A photocatalyst absorbs light and converts it to photogenerated charges that can be used to drive redox reactions on its surface. Most research has so far focused on photocatalysts fabricated from wide bandgap semiconductors such as $TiO_2$,[2,3] $SrTiO_3$,[4,5] and carbon nitride (CN).[6–8] However, photocatalysts fabricated from these semiconductors are primarily active under ultraviolet wavelengths, which contain <5% of solar energy.[1] This limits their maximum solar to hydrogen efficiency ($\eta_{STH}$) to

J. Kosco, C. T. Howells, W. Zhang, R. Sheelamanthula,  H. Faber,
B. Purushothaman, T. D. Anthopoulos, I. McCulloch
KAUST Solar Center (KSC)
Physical Sciences and Engineering Division (PSE)
King Abdullah University of Science and Technology (KAUST)
Thuwal 23955–6900, Kingdom of Saudi Arabia
E-mail: jan.kosco@kaust.edu.sa; iain.mcculloch@chem.ox.ac.uk
S. Gonzalez-Carrero, M. Sachs, J. R. Durrant
Department of Chemistry and Centre for Processable Electronics
Imperial College London
Exhibition Road, London SW7 2AZ, UK
M. Moser, B. Willner, I. McCulloch
Department of Chemistry
University of Oxford
12 Mansfield Road, Oxford OX1 4BH, UK

L. Zhao, R. Sougrat
KAUST Core Labs
King Abdullah University of Science and Technology (KAUST)
Thuwal 23955–6900, Kingdom of Saudi Arabia
T. C. Hidalgo, S. Inal
Biological and Environmental Science and Engineering Division
Organic Bioelectronics Laboratory
King Abdullah University of Science and Technology (KAUST)
Thuwal 23955–6900, Kingdom of Saudi Arabia
H. Cha
Department of Hydrogen and Renewable Energy
Kyungpook National University
Daegu 41566, Republic of Korea

**ADVANCED
SCIENCE NEWS**
www.advancedsciencenews.com

**ADVANCED
MATERIALS**
www.advmat.de

below the 5–10% threshold deemed necessary for commercial viability.[9] More recently, photocatalysts fabricated from a diverse range of organic semiconductors such as linear conjugated polymers,[10,11] crosslinked microporous polymers,[12–14] and covalent organic frameworks[14–17] have been developed.[18] The frontier molecular orbital energy levels of these semiconductors can be synthetically tuned to absorb a broader spectrum of solar irradiation while retaining suitable energy level alignments to drive the $H_2$ evolution reaction (HER) and/or the $O_2$ evolution reaction (OER). This enables them to achieve a maximum theoretical $\eta_{STH} > 10\%$.[1,18] Promising efficiencies have been achieved; however, further work is required to raise efficiencies toward this theoretical limit. Most studies that have focused on enhancing the photocatalytic $H_2$-evolution efficiency of organic semiconductor photocatalysts require the presence of sacrificial hole scavengers such as triethylamine (TEA) or ascorbic acid (AA).[11,19–21] These hole scavengers extract photogenerated holes from the semiconductor, which enables the photogenerated electrons to drive the HER. Some hole scavengers, such as high concentrations of TEA, can also facilitate charge separation at the semiconductor/electrolyte interface by extracting photogenerated holes directly from polymer excitons on the ps timescale.[11,20] This process is known as "reductive quenching" and is often the dominant mechanism of charge separation in photocatalysts composed of a single semiconductor.[22] Increasing the hydrophilicity of conjugated polymer photocatalysts through the incorporation of polar backbone units containing sulfone groups and/or hydrophilic glycol side chains has recently emerged as an effective strategy for improving photocatalytic efficiency.[20,23] Increased hydrophilicity makes the semiconductor more accessible to sacrificial hole scavengers which enhances charge separation via reductive quenching and can produce a concomitant increase in the photocatalyst's HER rate.[20,24]

Charge separation within an organic photocatalyst can also be induced by fabricating nanoparticle (NP) photocatalysts composed of a blend of two semiconductors with a type-II energy level offset. Exciton dissociation can occur at the electron donor/acceptor (D/A) heterojunction within the NPs which can enable D/A NPs to achieve greatly enhanced HER rates compared to NPs composed of the individual semiconductors.[18,21,25] Because exciton dissociation can take place inside the D/A NPs, these photocatalysts do not rely on reductive quenching by a hole scavenger to generate catalytically active charges. This enables them to operate efficiently even in the presence of lower concentration hole scavengers which extract holes from the semiconductor on the μs timescale, such as AA.[21] Furthermore, by using organic semiconductors with complementary absorptions, D/A NPs can be designed to absorb throughout the UV–visible spectrum.[26]

As well as enhancing hydrophilicity, the introduction of polar glycol side chains in conjugated polymers and fullerene derivatives has been shown to increase their relative permittivity (dielectric constant, $\varepsilon_r$).[27–29] This has been proposed to be responsible for reduced nongeminate recombination and increased charge-carrier lifetimes in bulk heterojunction (BHJ) solar cells, due to a reduced coulombic attraction between photogenerated polarons.[30] However, glycolation has not been shown to enhance charge generation or exciton dissociation in

conjugated polymers. This is possibly because glycol side chains cannot reorient fast enough to reduce the coulombic attraction between photogenerated electrons and holes in excitons (the exciton binding energy) before the excitons recombine.[31–33]

In this work, we explored the use of a range of conjugated polymers with glycol side chains in NP $H_2$-evolution photocatalysts. We demonstrate that glycolation greatly enhances the $H_2$-evolution rate of NP photocatalysts composed of the individual conjugated polymers and their blends with the electron acceptors $PC_{71}BM$ or oIDTBR. NP photocatalysts composed of a single glycolated semiconductor achieved greatly enhanced HER rates compared to their nonglycolated analogues. This HER rate enhancement occurred even when the glycolated and nonglycolated NPs had similar size distributions and when the relatively slow hole scavenger AA was used. Photophysical characterization revealed that glycolation can promote ultrafast charge separation and suppress both geminate and nongeminate recombination, leading to a higher yield of long-lived photogenerated charges within the glycolated NPs even in the absence of a D/A heterojunction, or the addition of Pt or a sacrificial hole scavenger. This was attributed to a higher $\varepsilon_r$ of the environment within the glycolated NPs, endowed by the high polarity of the glycol side chains and possibly also their hydrophilicity that enables the uptake of high-permittivity water molecules from the surrounding aqueous phase. NPs composed of a blend of an electron donor polymer and a small molecule electron acceptor introduced a D/A heterojunction within the NPs that further promoted exciton dissociation at the D/A interface. Glycolation of the donor polymer in these D/A NPs further reduced rates of geminate and nongeminate charge recombination. This increased the yield of long-lived polarons that remained within the NPs on timescales that enable $H_2$ evolution and hole scavenging by AA and led to a further dramatic enhancement of the HER rate.

## 2. Results

Analogues of the conjugated polymers indacenodithiophene–benzothiadiazole (IDTBT), poly(9,9-dioctylfluorene-*alt*-benzothiadiazole) (F8BT), and poly[4,8-bis(5-(2-ethylhexyl)thiophen-2-yl)benzo[1,2-b;4,5-b′]dithiophene-2,6-diyl-*alt*-(4-(2-ethylhexyl)-3-fluorothieno[3,4-b]thiophene-)-2-carboxylate-2-6-diyl)] (PTB7-Th) bearing either alkyl side chains (IDTBT, F8BT, PTB7-Th) or oligoethylene glycol side chains (gIDTBT, FgBT, gPTB7-Th) were synthesized (synthetic procedures can be found in the Supporting Information). These polymers were chosen because of their strong visible light absorption, solubility, and suitable highest occupied molecular orbital (HOMO) and lowest unoccupied molecular orbital (LUMO) energy levels (**Figure 1**). All the polymers had HOMO energy levels deep enough to drive ascorbic acid (AA) oxidation and LUMO levels shallow enough to drive proton reduction. Furthermore, they could also form a type-II electron donor/acceptor (D/A) heterojunction with at least one of the electron acceptors (oIDTBR or $PC_{71}BM$) used in this study.

NPs composed of the individual semiconductors and their blends with either oIDTBR or $PC_{71}BM$ were prepared using the miniemulsion method, and the NP size distributions were

**2105007** (2 of 9)
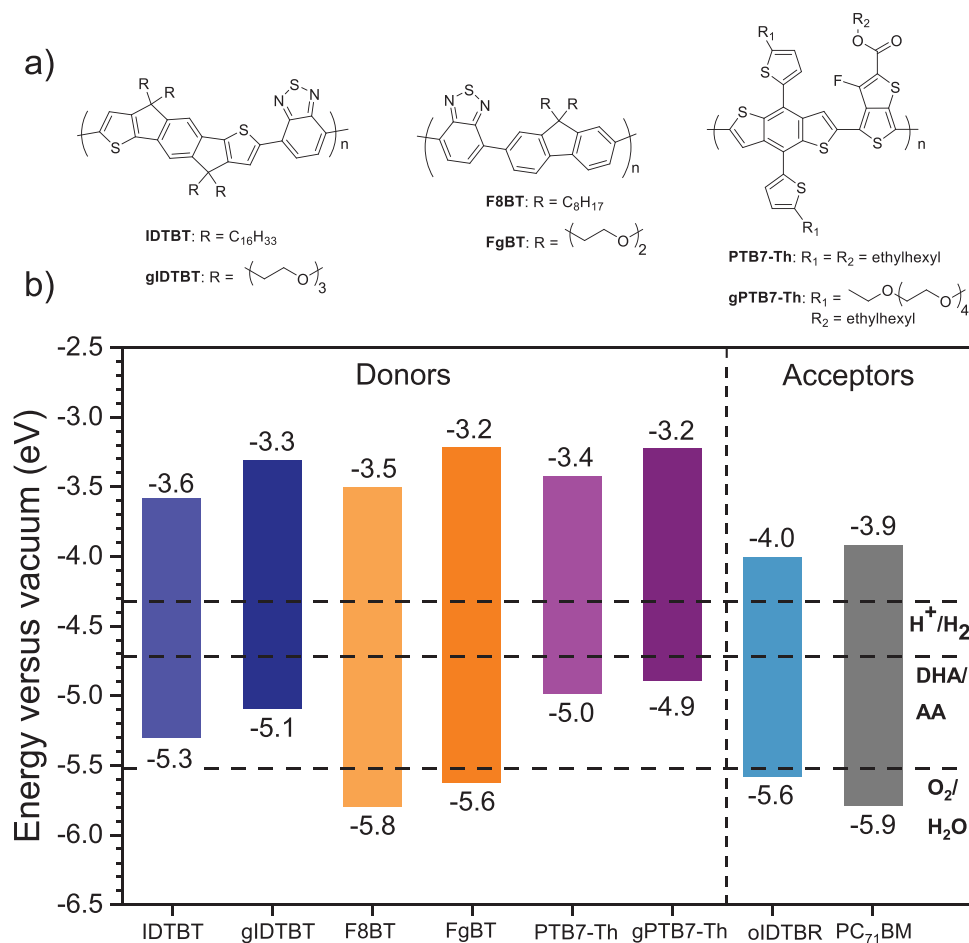
**Figure 1.** Chemical structures, energy levels, and absorption spectra. a) Chemical structures of IDTBT, gIDTBT, F8BT, FgBT, PTB7-Th, and gPTB7-Th. b) Frontier molecular orbital energy levels measured using a combination of photoelectron emission spectroscopy in air (PESA) and UV–visible absorption spectroscopy of dry films of IDTBT, gIDTBT, F8BT, FgBT, PTB7-Th, gPTB7-Th, and oIDTBR PC$_7$BM. The exciton binding energy is assumed to be negligible. The dashed lines correspond to the proton reduction potential (H$^+$/H$_2$), water oxidation potential (O$_2$/H$_2$O), and the calculated potential of the two-hole oxidation of ascorbic acid to dehydroascorbic acid in solution (DHA/AA) at pH 2 (the experimentally measured pH of 0.2 mol L$^{-1}$ ascorbic acid).[23] All energy levels and electrochemical potentials are expressed relative to vacuum (using −4.44 V vs vacuum = 0 V vs SHE).[34]

measured by dynamic light scattering (Figure S1, Tables S1–S3, Supporting Information).[35] The H$_2$-evolution rate of each NP batch was measured in the presence of photodeposited Pt, which served as a H$_2$-evolution co-catalyst, and the sacrificial hole scavenger AA (**Figure 2**).

Replacing alkyl side chains with glycol side chains increased the HER rate of NPs formed from gIDTBT by a factor of 16, of FgBT by a factor of 5, and of gPTB7-Th by a factor of 4 compared to their nonglycolated analogues (Figure 2a). These HER rate increases are comparable to those observed upon the replacement of alkyl side chains with glycol side chains in other conjugated polymers[20,29] and can be attributed to enhanced charge generation and increased polaron lifetimes in the glycolated semiconductors due to the increased $\varepsilon_r$ afforded by the glycol side chains, based on the analysis below. However, the HER rates of NPs composed of the individual semiconductors remained low. NPs composed of D/A blends (Figure 2b) achieved HER rates an order of magnitude higher than those composed of the individual donor polymers, and all D/A NPs that contained a glycolated semiconductor achieved a higher

HER rate than those containing their nonglycolated analogues. The highest HER rate of 4.21 µmol h$^{-1}$ cm$^{-2}$ (18.5 mmol h$^{-1}$ g$^{-1}$) over 16 h was achieved by the gIDTBT:oIDTBR NPs, which is a 30-fold increase compared to the nonglycolated IDTBT:oIDTBR NPs. An extended stability test (Figure 2c) revealed that the gIDTBT:oIDTBR NPs loaded with 10 wt% Pt could generate H$_2$ for ≥72 h, producing 1.1 mmol of H$_2$ in 72 h. They retained 93% of their original 24 h performance during the second 24 h cycle and 81% during the third 24 h cycle. Between cycles the reactor was evacuated, the NPs were removed from the reaction medium with the aid of a centrifugal filter and fresh AA was added (see the Supporting Information for details). The gIDTBT:oIDTBR NPs loaded with 10 wt% Pt were active throughout the visible spectrum and achieved photon-to-hydrogen conversion EQEs of ≈3% at 620–660 nm (Figure 2d). The greatest HER rate increase in NPs composed of the individual semiconductors and their blends was achieved upon the replacement of IDTBT with gIDTBT. Detailed functional characterization hereafter therefore focused primarily on the effect of replacing the alkyl side chains on IDTBT with glycol side
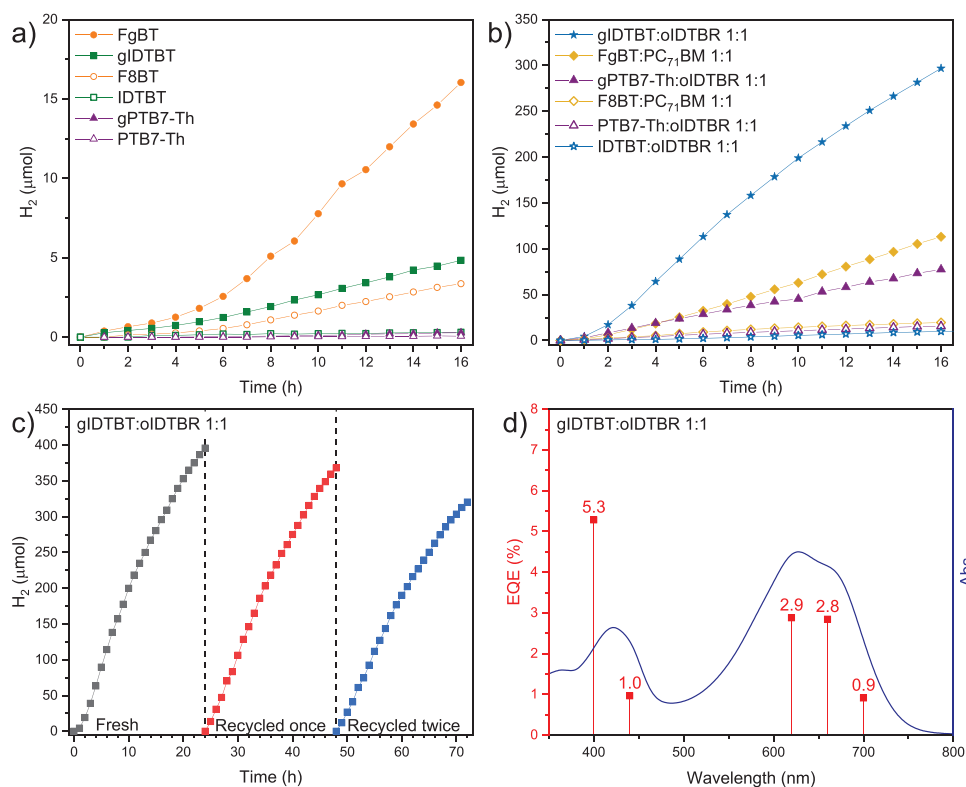
**Figure 2.** H$_2$ evolution and external quantum efficiencies (EQEs). a,b) H$_2$ evolution versus time of NPs composed of the individual donor polymers (a) and NPs containing a D/A heterojunction formed of a 1:1 blend by mass of a donor polymer matched with either oIDTBR or PC$_{71}$BM electron acceptors (b). Data presented are the average of three repeat runs. c) Stability and recyclability test of gIDTBT:oIDTBR NPs. Dashed lines indicate the times at which the reactor was evacuated to remove H$_2$ and the NPs were recycled. d) Absorption spectrum and EQEs of gIDTBT:oIDTBR NPs at 400, 440, 620, 660, and 700 nm. H$_2$-evolution conditions: 1 mg nanoparticles, 0.2 mol L$^{-1}$ ascorbic acid (12 mL), pH 2, 10 μg (10 wt%) Pt, AM1.5g solar simulator at 100 mW cm$^{-2}$ (1 sun), 4.41 cm$^2$ illumination area.

chains in NPs composed of the individual IDTBT and gIDTBT polymers and their blends with oIDTBR. As can be seen from Figure 2b,c, at longer times the HER rates become nonlinear. We have evaluated possible causes of this nonlinearity in detail, as shown in Figures S28–S30 (Supporting Information) and were able to rule out NP degradation, aggregation, or co-catalyst degradation. The primary cause of the nonlinearity appears to be AA depletion during the course of each run.

The NP morphology was characterized by cryogenic transmission electron microscopy (cryo-TEM, **Figure 3**). NPs formed of pure gIDTBT displayed an amorphous internal morphology, while oIDTBR NPs were highly crystalline with a periodic lattice spacing of ≈1.7 nm clearly visible as alternating lines of high and low electron density. This spacing corresponds to a diffraction peak at $q ≈ 0.41$ Å$^{-1}$ ($d = 15.3$ Å) observed by grazing-incidence X-ray diffraction in an annealed oIDTBR thin film.[36] The gIDTBT:oIDTBR NPs (Figure 3c) and the IDTBT:oIDTBR NPs (Figure 3e) both displayed a core–shell morphology with a crystalline oIDTBR core domain encapsulated by an amorphous IDTBT or gIDTBT shell. The oIDTBR domains retained their characteristic 1.7 nm lattice spacings, and the constant lattice orientation throughout the NP cores suggest that they are composed of a single oIDTBR crystal. The NP morphology was unchanged after 20 h H$_2$ evolution, and Pt was photodeposited in the form of NPs with a 2–5 nm diameter on both the

gIDTBT:oIDTBR NPs (Figure 3d) and the IDTBT:oIDTBR NPs (Figure 3e). The IDTBT:oIDTBR and the gIDTBT:oIDTBR NPs also had similar size distributions and the same 70 nm Z-average hydrodynamic diameter (Figure S1, Table S1, Supporting Information). From this it can be concluded that the enhanced HER rate of the gIDTBT:oIDTBR NPs did not originate from an improved NP morphology or a smaller particle size as has been reported previously for photocatalysts formed from a single glycolated semiconductor.[20,29]

To probe the photophysical origin of the increased HER rates in the NPs with glycol side chains, photoluminescence (PL) and transient absorption spectroscopy (TAS) were used, focusing on the effect of glycolating IDTBT. We first considered the effect of glycolation on neat polymer NPs. The PL spectrum of IDTBT NPs showed a broad emission with maximum at 725 nm; for gIDTBT NPs this emission is red shifted and six times lower in amplitude, indicating that glycolation strongly suppressed radiative exciton recombination (**Figure 4**a). Ultrafast transient absorption spectra for both IDTBT and gIDTBT NPs are shown in Figure 4b,c and Figure S7 (Supporting Information). For both NPs, the initial (1 ps) spectrum exhibits a ground state bleach at 670 nm (Figure S7, Supporting Information) and broad photoinduced absorption at 1300 nm, assigned to IDTBT singlet excitons, in agreement with previous studies of IDTBT films.[37] Interestingly, the NIR transient spectra of
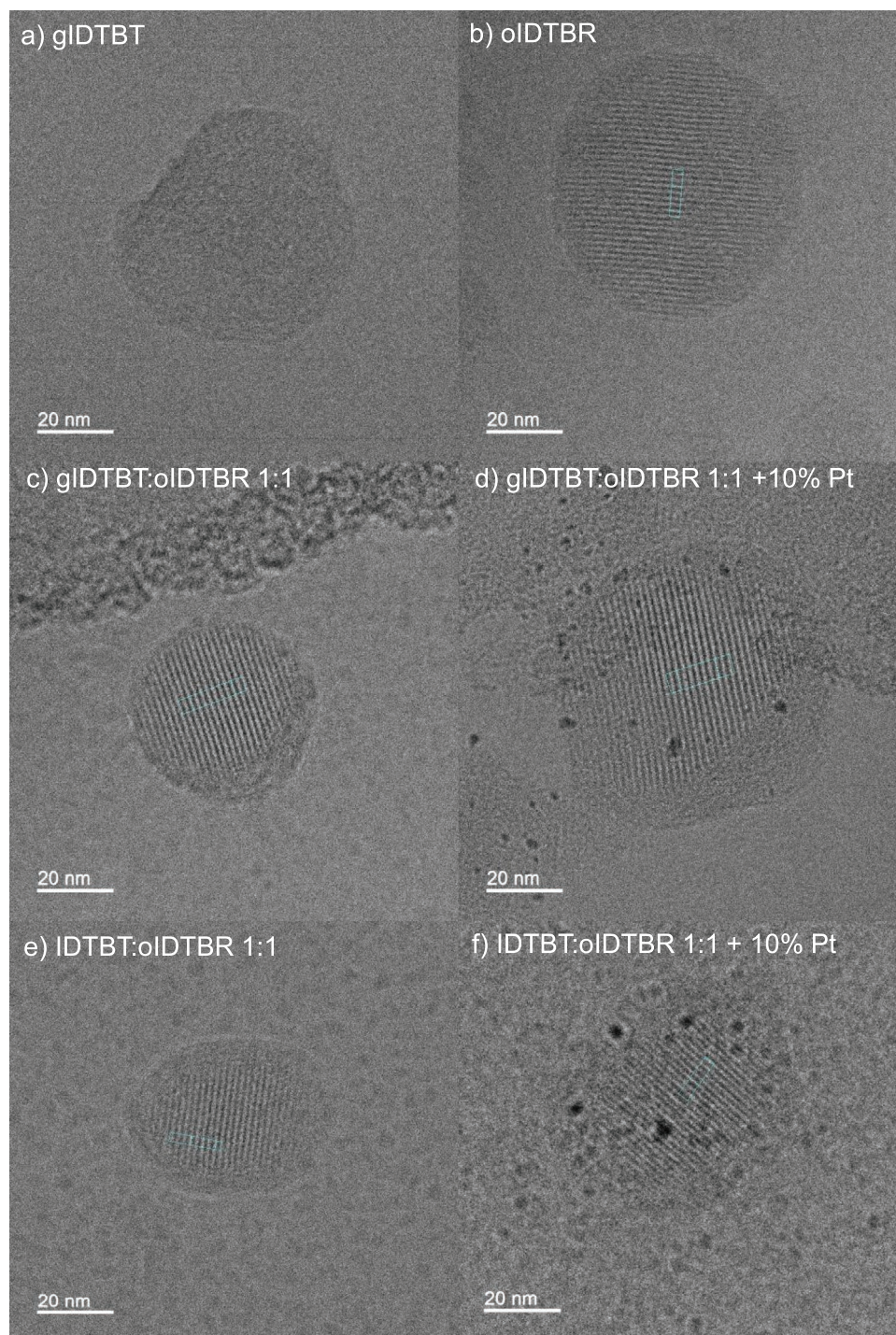
**Figure 3.** Bright-field cryo-TEM images of nanoparticles: a) gIDTBT, b) oIDTBR, c) gIDTBT:oIDTBR 1:1 before, and d) after photodeposition of 10 wt% Pt and 20 h $H_2$ evolution. e,f) IDTBT:oIDTBR 1:1 (e) before and after (f) photodeposition of 10 wt% Pt and 20 h $H_2$ evolution. Profiles of the periodic spacings in the rectangles in images (b)–(f) are available in Figures S4–S6 (Supporting Information). Note: The dark areas at the top of images (c) and (d) originate from the TEM grid.

gIDTBT evolve into a band with a maximum at 1050 nm over the first 100 ps; this band is much less pronounced for nonglycolated IDTBT NPs. This 1050 nm absorption feature was also observed in transient spectra of gIDTBT NPs at longer time scales (μs–ms), exhibiting power-law decay kinetics and slow

quenching by molecular oxygen, indicative of its assignment to long-lived gIDTBT polarons. (Figures S8 and S9, Supporting Information). In contrast, for nonglycolated IDTBT NPs, only a low amplitude, shorter lived (μs) and strongly oxygen quenched absorption signal was observed, indicative of IDTBT triplet
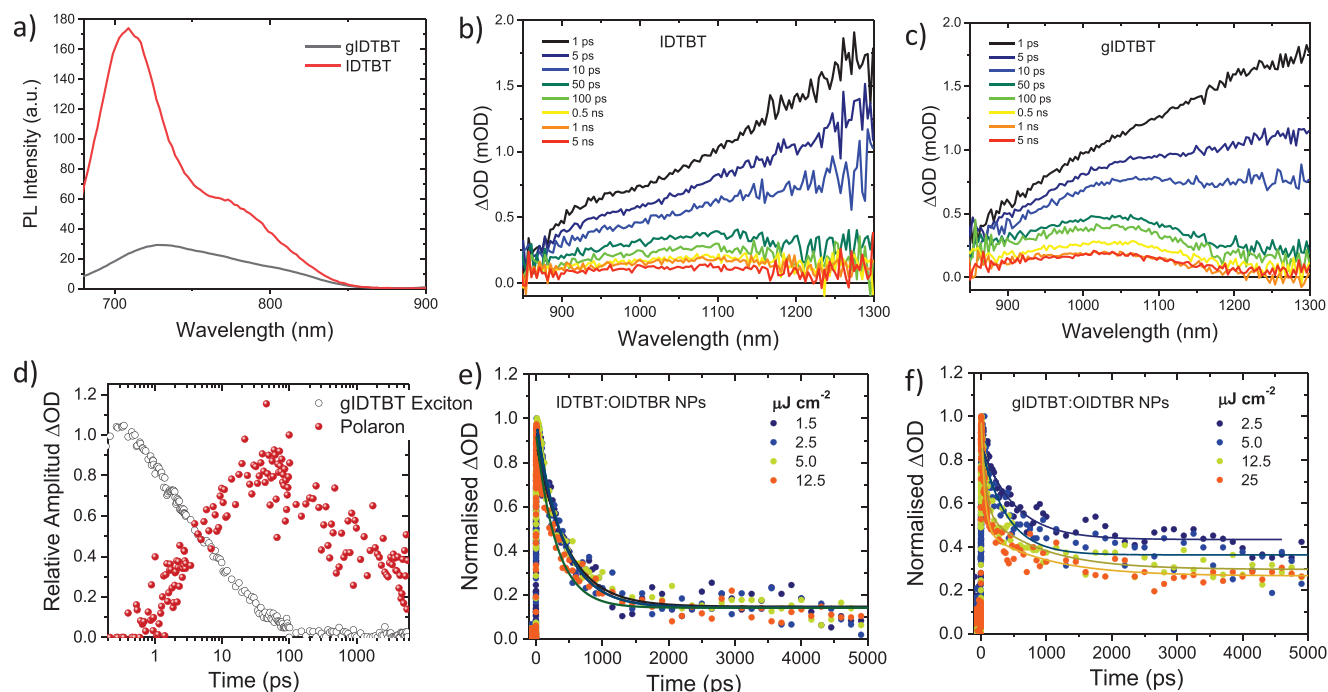
**Figure 4.** Photophysics of NPs in aqueous suspension. a) Steady-state photoluminescence spectra of gIDTBT and IDTBT NP suspensions, excited at 650 nm. b,c) Ultrafast transient absorption spectra of IDTBT and gIDTBT NP suspensions at different delay times. d) Deconvoluted transient absorption kinetics of gIDTBT excitons and polarons obtained via global analysis (see the Supporting Information for details) of the data shown in (c). e,f) Transient absorption kinetics representing polaron decay kinetics at different fluences in IDTBT:oIDTBR and gIDTBT:oIDTBR NP suspensions, probed at 750 nm. Full lines are monoexponential fits to the data with an offset. All transient absorption data were recorded following 650 nm excitation using a fluence of 5 μJ cm$^{-2}$ unless indicated otherwise.

excitons (Figure S9, Supporting Information).[38] Deconvolution of the exciton and polaron signals observed for gIDTBT NPs on ultrafast timescales indicates the formation of this polaron signal with a 8 ps halftime, concomitant with the decay of gIDTBT singlet excitons (Figure 4d), indicative of rapid charge generation, and consistent with the strongly suppressed PL of gIDTBT NPs. This polaron signal was observed to exhibit a fluence-independent decay with a half time of ≈1 ns (Figure S10, Supporting Information), indicative of a significant proportion of geminate recombination of bound charge pairs (i.e., intermolecular charge transfer states). These results indicate that the modification of IDTBT with glycol side chains results in surprisingly efficient exciton separation even in the absence of a D/A heterojunction, or the addition of Pt or a sacrificial hole scavenger. The enhanced charge generation in the gIDTBT NPs results in a higher yield of catalytically active charges and is responsible for their enhanced HER rate compared to their nonglycolated analogues.

We now focus on transient absorption studies of the exciton and polaron kinetics in D/A NPs with oIDTBR (Figure 4e,f; Figures S11–S15, Supporting Information). For both IDTBT:oIDTBR and gIDTBT:oIDTBR NPs, singlet exciton signals were strongly quenched within 1 ps, with polaron absorption at 1050 nm dominating the NIR transient spectra, indicative of efficient, sub-picosecond exciton separation to form charges in both NPs. However, the two NPs differ significantly in the decay dynamics of these charges. IDTBT:oIDTBR NPs showed a rapid (≈500 ps) and fluence-independent decay kinetics, indicative of the geminate (monomolecular) recombination of

photogenerated charge transfer (CT) states, with only a low yield (≈10%) of long-lived, separated charges. Analogous, field-dependent geminate recombination losses have been observed in organic photovoltaic devices employing oIDTBR, and were attributed to a small energy offset and morphological effects.[39,40] In contrast, gIDTBT:oIDTBR NPs exhibited slower, fluence dependent decay kinetics, indicative of the bimolecular recombination of spatially separated polarons, and indicating that glycolation results in the strong suppression of CT state geminate recombination. μs–ms transient absorption data indicate a higher yield of longer lived charges in gIDTBT:oIDTBR NPs compared to IDTBT:oIDTBR NPs (Figure S15, Supporting Information), further confirming that glycolation results in a retardation of charge recombination losses. It can be concluded that glycolation substantially enhances the efficiency of charge separation in these D/A NPs, which is consistent with the observed higher rates of H$_2$ evolution.

The data shown in Figure 4 indicate that glycolation results in a substantive suppression of exciton and polaron recombination in these NPs. This effect is observed even in neat gIDTBT NPs, which exhibit remarkably efficient charge generation. However, in the absence of a D/A heterojunction, the charges generated primarily undergo geminate recombination on the nanosecond timescale. This is too fast for efficient hole scavenging by AA, which is consistent with the low H$_2$ yield from NPs composed of pure gIDTBT. In the gIDTBT:oIDTBR and the IDTBT:oIDTBR NPs, exciton separation is efficient both with and without glycolation due to the presence of a D/A heterojunction within the NPs. The effect of glycolation in the

**ADVANCED
SCIENCE NEWS**

www.advancedsciencenews.com

**ADVANCED
MATERIALS**

www.advmat.de
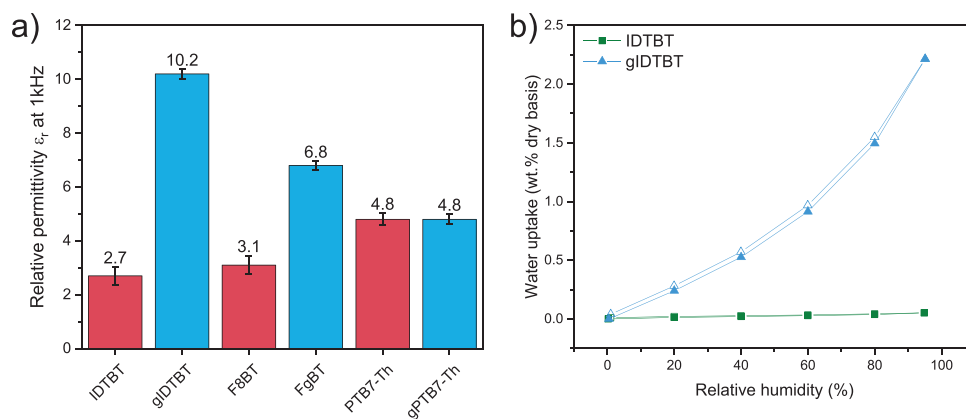
**Figure 5.** Relative permittivities and water uptake. a) Relative permittivity at 1 kHz of dry films of the donor polymers used in this study. b) Water vapor adsorption isotherms of IDTBT and gIDTBT. Full symbols represent adsorption and empty symbols represent desorption.

gIDTBT:oIDTBR NPs is primarily to suppress both geminate and nongeminate recombination. The resultant generation of long-lived charges enables efficient hole scavenging by AA on the µs timescale (Figure S15, Supporting Information), and the remarkably efficient photocatalytic $H_2$ evolution of the gIDTBT:oIDTBR NPs compared to their nonglycolated analogues. These data also confirm that the enhanced HER rates of the glycolated NPs did not originate simply from an increased availability of their hydrophilic surface to AA, because AA does not extract holes from the NPs on a timescale fast enough to efficiently dissociate polymer excitons. Hole extraction by AA takes place on the µs timescale (Figure S15, Supporting Information), which is several orders of magnitude slower than the typical timescale of singlet exciton recombination in organic semiconductors (ps–ns).[11,20,22] Rather, glycolation results in a higher yield of long-lived photogenerated charges capable of driving AA oxidation and $H_2$ evolution.

Glycolation has also been reported to enhance the performance of dibenzo[b,d]thiophene sulfone polymer photocatalyst dispersions, attributed to a higher wettability and an increased local dielectric aiding charge stabilization, consistent with the results herein. However with this sulfone polymer, long-lived charge generation was only observed in the presence of 30% TEA, with glycolation increasing the efficiency hole scavenging,[20] as well as increasing the lifetime of the resultant electron polarons. The results herein indicate that glycolation can enhance the charge separation and retard charge recombination of the polymer NPs even in the absence of a sacrificial electron donor, by impacting on the intrinsic, ultrafast photophysics of these NPs. This impact of glycolation on the ultrafast exciton and charge dynamics is particularly striking, and contrasts with studies of the impact of glycolation on spin coated, dry polymer films and BHJs, where extensive studies have reported impact only on slower (typically ns–ms) charge-carrier dynamics,[27,31,32,41,42] as discussed further below.

Suppressed charge recombination has been reported when glycolated semiconductors were used in organic solar cells, as a result of their enhanced relative permittivities compared to their nonglycolated analogues.[43–45] An increased $\varepsilon_r$ reduces the coulombic attraction between photogenerated electrons and holes and can result in reduced recombination and longer charge-carrier lifetimes in organic semiconductor films.[30,45] Measuring the $\varepsilon_r$ of the polymers used in this study (**Figure 5**a) in dry films revealed that glycolation increased the $\varepsilon_r$ of gIDTBT by a factor of 2.7, of FgBT by a factor of 1.6, and of gPTB7-Th by a negligible amount compared to their nonglycolated analogues. These increases in relative permittivity can be attributed to the presence of C—O dipoles on the glycol side chains which can readily reorient in response to an electric field and thus better shield coulombic fields between photogenerated charges.[27] Only three out of the four alkyl side chains on the PTB7-Th repeat unit were replaced with glycol side chains in gPTB7-Th, which may be why glycolation only resulted in a negligible increase of the $\varepsilon_r$ of gPTB7-Th compared to PTB7-Th.

Glycolation of single conjugated polymers has been shown to increase the polymers' affinity to water, with lower water contact angles and higher water adsorption compared to their alkyl side chain analogues.[20] Here, glycolation was also found to enhance the hydrophilicity of all three conjugated polymers, as evidenced by the lower water contact angles of gIDTBT, FgBT, and gPTB7-Th (67°, 86°, and 79°, respectively) compared to IDTBT, F8BT, and PTB7-Th (105°, 99°, and 108°, respectively) (Figure S16, Table S4, Supporting Information). Furthermore, dynamic water vapor sorption measurements (Figure 5b) revealed that glycolation greatly increased the ability of gIDTBT to adsorb water. At 95% relative humidity, the hydrophilic gIDTBT polymer achieved a water vapor uptake of 2.2% compared to just 0.05% for IDTBT, a more than 40-fold enhancement. The type-III gIDTBT water adsorption isotherm displays an exponential increase in water uptake with increasing relative humidity that is characteristic of multi-layer adsorption.[46,47] Quartz crystal microbalance measurements on thin films of IDTBT and gIDTBT (Figure S19, Supporting Information) revealed that upon immersion in water (or 0.2 M AA), the mass of gIDTBT increased by 120%. This suggests that the ingress of liquid water into the hydrophilic gIDTBT film caused the polymer to swell.[20,48] The mass of the IDTBT film also increased upon water immersion although, with a mass increase of only 20%, by substantially less than the gIDTBT film. Nevertheless, this is surprisingly high considering the hydrophobicity and low water vapor uptake of IDTBT. It is therefore likely that this relatively small mass increase originated

from voids in the IDTBT film being filled by water, as has been previously reported,[49] rather than by water swelling the film. This is supported by atomic force microscopy measurements (Figure S20, Supporting Information) which show a negligible increase in the thickness of an IDTBT film upon water immersion, compared to an 11% increase for a gIDTBT film.

Glycolation of dry organic semiconductor films typically only affects their low frequency (up to 1 MHz) dielectric response.[32] Therefore, in dry organic semiconductor films, glycolation can retard charge recombination mechanisms that take place on the µs timescale, such as nongeminate recombination, but typically has little impact on exciton and charge-transfer state separation, which take place on the ps–ns timescale.[32,45] However, the observation that glycolation of our NP photocatalysts in water enhances exciton/charge transfer state separation, both in the presence and absence of a D/A heterojunction, suggests that glycolation of these NPs also enhances their high-frequency (GHz) relative permittivity. This can most likely be related to the enhanced water uptake of these NPs.[20] Water retains a relative permittivity of >50 at frequencies up to 10 GHz, and 7–8 at frequencies up to 1 THz.[50] The presence of water molecules in the polymer matrix could therefore yield an enhanced high-frequency dielectric response, capable of reducing the coulomb attraction of both excitons and charge transfer states on the ps–ns timescale.[50,51] While further work is necessary to confirm this, it is apparent that the enhanced generation of long-lived charges observed with glycolation correlates with the enhanced $H_2$-evolution rates of glycolated NP photocatalysts.

## 3. Conclusion

We have demonstrated that glycolation is an effective strategy to enhance the photocatalytic efficiency of NP $H_2$-evolution photocatalysts. The strategy is broadly applicable to a range of structurally diverse conjugated polymers. In NP photocatalysts composed of a single semiconductor, glycolation suppresses exciton recombination and increases the efficiency of intrinsic charge generation within the NPs, which increases their HER rate compared to NPs composed of their nonglycolated analogues. However, in NPs composed of a single semiconductor, most of these charges decay via geminate recombination on the nanosecond timescale, too fast for efficient hole scavenging by AA, which limits their $H_2$-evolution efficiency. Fabricating NPs composed of two semiconductors with a type-II energy level offset introduces a D/A heterojunction within the NPs that efficiently dissociates excitons at the D/A interface. Glycolation of the donor polymer in these NPs suppresses both geminate and nongeminate recombination. The resultant generation of long-lived charges within the glycolated D/A NPs enables efficient hole scavenging by AA, which greatly enhances their photocatalytic $H_2$-evolution rate. The effectiveness of glycol side chains in suppressing the ps–ns exciton and charge transfer state recombination losses observed for our neat and D/A NPs herein is remarkable, suggesting an impact of glycolation on the high-frequency (GHz) permittivity of our NPs. The effectiveness of glycolation in suppressing such ps–ns recombination in our NPs may be associated with the hydrophilicity and small size of these NPs, facilitating the ingress of highly polar water

molecules into these NPs, and thus substantially increasing the effective dielectric response of these NPs on a timescale fast enough to screen the coulomb attraction of excitons and CT states.[50,51]

## 4. Experimental Section

Details of the experimental methods can be found in the Supporting Information.

## Supporting Information

Supporting Information is available from the Wiley Online Library or from the author.

## Conflict of Interest

The authors declare no conflict of interest.

## Data Availability Statement

The data that support the findings of this study are available from the corresponding author upon reasonable request.

[1] Q. Wang, K. Domen, *Chem. Rev.* **2020**, *120*, 919.
[2] J. Schneider, M. Matsuoka, M. Takeuchi, J. Zhang, Y. Horiuchi, M. Anpo, D. W. Bahnemann, *Chem. Rev.* **2014**, *114*, 9919.
[3] M. Ni, M. K. H. Leung, D. Y. C. Leung, K. Sumathy, *Renewable Sustainable Energy Rev.* **2007**, *11*, 401.
[4] P. Yohan, H. Takashi, D. Kazunari, in *Current Developments in Photocatalysis and Photocatalytic Materials*, Elsevier, Amsterdam, The Netherlands **2020**, pp. 141–157.

[5] T. Takata, J. Jiang, Y. Sakata, M. Nakabayashi, N. Shibata, V. Nandal, K. Seki, T. Hisatomi, K. Domen, *Nature* **2020**, *581*, 411.

[6] G. Zhang, L. Lin, G. Li, Y. Zhang, A. Savateev, S. Zafeiratos, X. Wang, M. Antonietti, *Angew. Chem., Int. Ed.* **2018**, *57*, 9372.

[7] S. Yang, Y. Gong, J. Zhang, L. Zhan, L. Ma, Z. Fang, R. Vajtai, X. Wang, P. M. Ajayan, *Adv. Mater.* **2013**, *25*, 2452.

[8] X. Wang, K. Maeda, A. Thomas, K. Takanabe, G. Xin, J. M. Carlsson, K. Domen, M. Antonietti, *Nat. Mater.* **2009**, *8*, 76.

[9] B. A. Pinaud, J. D. Benck, L. C. Seitz, A. J. Forman, Z. Chen, T. G. Deutsch, B. D. James, K. N. Baum, G. N. Baum, S. Ardo, H. Wang, E. Miller, T. F. Jaramillo, *Energy Environ. Sci.* **2013**, *6*, 1983.

[10] S. Yanagida, A. Kabumoto, K. Mizumoto, C. Pac, K. Yoshino, *J. Chem. Soc., Chem. Commun.* **1985**, 474.

[11] M. Sachs, R. S. Sprick, D. Pearce, S. A. J. Hillman, A. Monti, A. A. Y. Guilbert, N. J. Brownbill, S. Dimitrov, X. Shi, F. Blanc, M. A. Zwijnenburg, J. Nelson, J. R. Durrant, A. I. Cooper, *Nat. Commun.* **2018**, *9*, 4968.

[12] F. Vilela, K. Zhang, M. Antonietti, *Energy Environ. Sci.* **2012**, *5*, 7819.

[13] P. Guiglion, C. Butchosa, M. A. Zwijnenburg, *Macromol. Chem. Phys.* **2016**, *217*, 344.

[14] V. S. Vyas, V. W. Lau, B. V. Lotsch, *Chem. Mater.* **2016**, *28*, 5191.

[15] F. Beuerle, B. Gole, *Angew. Chem., Int. Ed.* **2018**, *57*, 4850.

[16] T. Banerjee, K. Gottschling, G. Savasci, C. Ochsenfeld, B. V. Lotsch, *ACS Energy Lett.* **2018**, *3*, 400.

[17] X. Feng, X. Ding, D. Jiang, *Chem. Soc. Rev.* **2012**, *41*, 6010.

[18] J. Kosco, F. Moruzzi, B. Willner, I. McCulloch, *Adv. Energy Mater.* **2020**, *10*, 2001935.

[19] Y. Bai, L. Wilbraham, B. J. Slater, M. A. Zwijnenburg, R. S. Sprick, A. I. Cooper, *J. Am. Chem. Soc.* **2019**, *141*, 9063.

[20] D. J. Woods, S. A. J. Hillman, D. Pearce, L. Wilbraham, L. Q. Flagg, W. Duffy, I. McCulloch, J. R. Durrant, A. A. Y. Guilbert, M. A. Zwijnenburg, R. S. Sprick, J. Nelson, A. I. Cooper, *Energy Environ. Sci.* **2020**, *13*, 1843.

[21] J. Kosco, M. Bidwell, H. Cha, T. Martin, C. T. Howells, M. Sachs, D. H. Anjum, S. G. Lopez, L. Zou, A. Wadsworth, W. Zhang, L. Zhang, J. Tellam, R. Sougrat, F. Laquai, D. M. DeLongchamp, J. R. Durrant, I. McCulloch, *Nat. Mater.* **2020**, *19*, 559.

[22] M. Sachs, H. Cha, J. Kosco, C. M. Aitchison, L. Francàs, S. Corby, C. L. Chiang, A. A. Wilson, R. Godin, A. Fahey-Williams, A. I. Cooper, R. S. Sprick, I. McCulloch, J. R. Durrant, *J. Am. Chem. Soc.* **2020**, *142*, 14574.

[23] X. Wang, L. Chen, S. Y. Chong, M. A. Little, Y. Wu, W.-H. Zhu, R. Clowes, Y. Yan, M. A. Zwijnenburg, R. S. Sprick, A. I. Cooper, *Nat. Chem.* **2018**, *10*, 1180.

[24] Y. Wang, A. Vogel, M. Sachs, R. S. Sprick, L. Wilbraham, S. J. A. Moniz, R. Godin, M. A. Zwijnenburg, J. R. Durrant, A. I. Cooper, J. Tang, *Nat. Energy* **2019**, *4*, 746.

[25] A. Wadsworth, Z. Hamid, J. Kosco, N. Gasparini, I. McCulloch, *Adv. Mater.* **2020**, *32*, 2001763.

[26] A. Liu, L. Gedda, M. Axelsson, M. Pavliuk, K. Edwards, L. Hammarström, H. Tian, *J. Am. Chem. Soc.* **2021**, *143*, 2875.

[27] S. Torabi, F. Jahani, I. Van Severen, C. Kanimozhi, S. Patil, R. W. A. Havenith, R. C. Chiechi, L. Lutsen, D. J. M. Vanderzande, T. J. Cleij, J. C. Hummelen, L. J. A. Koster, *Adv. Funct. Mater.* **2015**, *25*, 150.

[28] B. Meng, J. Liu, L. Wang, *Polym. Chem.* **2020**, *11*, 1261.

[29] Z. Hu, Z. Wang, X. Zhang, H. Tang, X. Liu, F. Huang, Y. Cao, *iScience* **2019**, *13*, 33.

[30] N. Cho, C. W. Schlenker, K. M. Knesting, P. Koelsch, H. L. Yip, D. S. Ginger, A. K. Y. Jen, *Adv. Energy Mater.* **2014**, *4*, 1301857.

[31] A. A. Mohapatra, Y. Dong, P. Boregowda, A. Mohanty, A. Sadhanala, X. Jiao, A. Narayan, C. R. McNeill, J. R. Durrant, S. Patil, *J. Phys. Chem. C* **2021**, *125*, 6896.

[32] S. Sami, R. Alessandri, R. Broer, R. W. A. Havenith, *ACS Appl. Mater. Interfaces* **2020**, *12*, 17783.

[33] N. Koizumi, T. Hanai, *J. Phys. Chem.* **1956**, *60*, 1496.

[34] S. Trasatti, *J. Electroanal. Chem. Interfacial Electrochem.* **1986**, *209*, 417.

[35] K. Landfester, *Adv. Mater.* **2001**, *13*, 765.

[36] S. Holliday, R. S. Ashraf, A. Wadsworth, D. Baran, S. A. Yousaf, C. B. Nielsen, C.-H. Tan, S. D. Dimitrov, Z. Shang, N. Gasparini, M. Alamoudi, F. Laquai, C. J. Brabec, A. Salleo, J. R. Durrant, I. McCulloch, *Nat. Commun.* **2016**, *7*, 11585.

[37] T. H. Thomas, D. J. Harkin, A. J. Gillett, V. Lemaur, M. Nikolka, A. Sadhanala, J. M. Richter, J. Armitage, H. Chen, I. McCulloch, S. M. Menke, Y. Olivier, D. Beljonne, H. Sirringhaus, *Nat. Commun.* **2019**, *10*, 2614.

[38] Y. W. Soon, S. Shoaee, R. S. Ashraf, H. Bronstein, B. C. Schroeder, W. Zhang, Z. Fei, M. Heeney, I. McCulloch, J. R. Durrant, *Adv. Funct. Mater.* **2014**, *24*, 1474.

[39] D. Baran, N. Gasparini, A. Wadsworth, C. H. Tan, N. Wehbe, X. Song, Z. Hamid, W. Zhang, M. Neophytou, T. Kirchartz, C. J. Brabec, J. R. Durrant, I. McCulloch, *Nat. Commun.* **2018**, *9*, 2059.

[40] C.-H. Tan, A. Wadsworth, N. Gasparini, S. Wheeler, S. Holliday, R. S. Ashraf, S. D. Dimitrov, D. Baran, I. McCulloch, J. R. Durrant, *J. Phys. Chem. C* **2019**, *123*, 5826.

[41] N. Cho, C. W. Schlenker, K. M. Knesting, P. Koelsch, H.-L. Yip, D. S. Ginger, A. K.-Y. Jen, *Adv. Energy Mater.* **2014**, *4*, 1301857.

[42] G. Zhang, T. M. Clarke, A. J. Mozer, *J. Phys. Chem. C* **2016**, *120*, 7033.

[43] M. Lenes, F. B. Kooistra, J. C. Hummelen, I. Van Severen, L. Lutsen, D. Vanderzande, T. J. Cleij, P. W. M. Blom, *J. Appl. Phys.* **2008**, *104*, 114517.

[44] X. Chen, Z. Zhang, Z. Ding, J. Liu, L. Wang, *Angew. Chem., Int. Ed.* **2016**, *55*, 10376.

[45] J. Brebels, J. V. Manca, L. Lutsen, D. Vanderzande, W. Maes, *J. Mater. Chem. A* **2017**, *5*, 24037.

[46] A. Nistor, G. Stiubianu, C. Racles, M. Cazacu, *Mater. Plast. (Bucharest, Rom.)* **2011**, *48*, 33.

[47] K. C. Ng, M. Burhan, M. W. Shahzad, A. Bin Ismail, *Sci. Rep.* **2017**, *7*, 10634.

[48] M. Moser, T. C. Hidalgo, J. Surgailis, J. Gladisch, S. Ghosh, R. Sheelamanthula, Q. Thiburce, A. Giovannitti, A. Salleo, N. Gasparini, A. Wadsworth, I. Zozoulenko, M. Berggren, E. Stavrinidou, S. Inal, I. McCulloch, *Adv. Mater.* **2020**, *32*, 2002748.

[49] M. Nikolka, I. Nasrallah, B. Rose, M. K. Ravva, K. Broch, A. Sadhanala, D. Harkin, J. Charmet, M. Hurhangee, A. Brown, S. Illig, P. Too, J. Jongman, I. McCulloch, J. L. Bredas, H. Sirringhaus, *Nat. Mater.* **2017**, *16*, 356.

[50] A. Andryieuski, S. M. Kuznetsova, S. V. Zhukovsky, Y. S. Kivshar, A. V. Lavrinenko, *Sci. Rep.* **2015**, *5*, 13535.

[51] N. Shinyashiki, S. Sudo, W. Abe, S. Yagihara, *J. Chem. Phys.* **1998**, *109*, 9843.